The Pseudomonas aeruginosa exotoxin A translocation domain facilitates the routing of CPP–protein cargos to the cytosol of eukaryotic cells

ARTICLE *in* JOURNAL OF CONTROLLED RELEASE · OCTOBER 2012

Impact Factor: 7.71 · DOI: 10.1016/j.jconrel.2012.10.006 · Source: PubMed

7 AUTHORS, INCLUDING:

Eric H-B Huang

14 PUBLICATIONS **116** CITATIONS

SEE PROFILE

Marzena Cydzik

Sunnybrook Health Sciences Centre

12 PUBLICATIONS **57** CITATIONS

SEE PROFILE

Journal of Controlled Release 164 (2012) 58–64

Contents lists available at SciVerse ScienceDirect

Journal of Controlled Release

journal homepage: www.elsevier.com/locate/jconrel

The *Pseudomonas aeruginosa* exotoxin A translocation domain facilitates the routing of CPP–protein cargos to the cytosol of eukaryotic cells

Arshiya F. Mohammed [a,c], Aws Abdul-Wahid [a,c], Eric H.-B. Huang [c], Eleonora Bolewska-Pedyczak [c], Marzena Cydzik [c], Amaalia E. Broad [b], Jean Gariépy [a,b,c,*]

[a] Department of Medical Biophysics, University of Toronto, Toronto, Ontario, Canada
[b] Department of Pharmaceutical Sciences, University of Toronto, Toronto, Ontario, Canada
[c] Physical Sciences, Sunnybrook Research Institute, Toronto, Ontario, Canada

ARTICLE INFO

Article history:
Received 30 August 2012
Accepted 8 October 2012
Available online 14 October 2012

Keywords:
Cell penetrating peptide
Exotoxin A translocation domain
Cellular internalization
Delivery of protein therapeutics
Endosomal escape

ABSTRACT

The use of cell-penetrating peptides (CPPs), such as polyarginine, has been shown to facilitate the import of drugs and other cargos into cells. However, a major obstacle limiting their use as delivery agents is their entrapment following internalization into endocytic vesicles, leading to either their recycling out of cells or their degradation in lysosomes. To address this challenge, we fused a CPP sequence to the translocation domain of *Pseudomonas aeruginosa* exotoxin A (ETA) to facilitate the endosomal escape of imported CPP-containing protein constructs. Specifically, a fusion protein incorporating ten arginines linked to residues 253 to 412 of ETA ($ETA^{253–412}$) was tested for its ability to effectively route a protein cargo (enhanced green fluorescent protein, eGFP) to the cytosol of cells. Using flow cytometry and fluorescence live-cell imaging, we observed a 5-fold improvement of cellular uptake as well as a 40-fold increase in cytosolic delivery of the CPP–$ETA^{253–412}$–eGFP construct in relation to CPP–eGFP. Furthermore, analysis of intracellular routing events indicated that the incorporation of $ETA^{253–412}$ within the CPP-containing protein fusion construct avoided lysosomal degradation by re-directing the construct from early endosomes to the ER lumen and finally to the cytosol. Studies using inhibitors of vesicular transport confirmed that the ER lumen is a key compartment reached by the CPP–$ETA^{253–412}$–eGFP construct before accessing the cytosol. Together, these findings suggest that incorporating a CPP motif and the ETA translocation domain into protein constructs can facilitate their cytosolic delivery.

1. Introduction

Cell penetrating peptides (CPPs), also known as protein transduction domains (PTDs), are small peptide sequences, 8 to 30 amino acids in length, that allow the internalization of charged macromolecules via proteoglycan-dependent mechanisms [1,2]. Polycationic CPPs represent a major class of cell penetrating peptides exemplified by arginine-rich peptides such as poly-arginine (R_n, where $n \geq 8$) and the related HIV-1 TAT peptide, a peptide derived from the transduction domain of the human immunodeficiency virus type 1 transactivator of transcription protein (RKKRRQRRR, amino acids 49–57) [1,3]. Mechanistically, cationic CPPs bind to negatively charged cell surface proteoglycans (PGs) such as heparin sulfate proteoglycans (HSPGs) via electrostatic interactions [1,3]. HSPGs act as multivalent low affinity receptors and internalize bound CPPs through endocytic pathways such as macropinocytosis or clathrin-mediated endocytosis [1,3].

Despite their clinical potential, the use of CPPs has been hampered by the fact that their internalized cargos remain mostly trapped in endocytic vesicles, leading to their subsequent degradation or recycling out of cells [1,3]. Endosomal entrapment leads to a substantial reduction (to less than 1%) in the amount of CPP-delivered cargos reaching targets residing in the cytosol or other subcellular compartments [4–8]. To address this routing limitation, we proposed the use of the known translocation domain of the bacterial protein exotoxin A (ETA) as a potential endosomal escape function in building CPP-delivered protein cargos.

ETA is a single chain (66.6 kD) protein toxin secreted by pathogenic *Pseudomonas aeruginosa* bacteria. Structurally, ETA is subdivided into three functional modules. Domain Ia (residues 1–252) is responsible for the binding of the toxin to its cognate receptor (α2 macroglobulin receptor/low density lipoprotein receptor) on target cells, leading to its internalization [9]. Domain II (residues 253–364) facilitates the translocation of ETA from either endosomes or the ER lumen to the cytoplasm. Importantly, the deletion of domain II or mutations within this domain results in a significant loss of cytotoxicity [10–13]. Domain Ib (residues 365–404) is thought to serve as a spacer between domains II and III [14]. Lastly, domain III (residues 405–613) contains the catalytic function by which ETA blocks protein synthesis and causes cell death

* Corresponding author at: University of Toronto, Physical Sciences Discipline, Sunnybrook Research Institute, M7-434, Sunnybrook Health Sciences Centre, 2075 Bayview Avenue, Toronto, Ontario, Canada M4N 3M5. Tel.: +1 416 480 5710; fax: +1 416 480 5714.
E-mail address: gariepy@sri.utoronto.ca (J. Gariépy).

0168-3659/$ – see front matter © 2012 Elsevier B.V. All rights reserved.
http://dx.doi.org/10.1016/j.jconrel.2012.10.006

[15]. Previous studies have focused on the use of various domains of ETA to create targeted chimeric toxins. Specifically, domain I has been replaced with different ligands including transforming growth factor type alpha (TGF-α), interleukin 4, as well as antibody domains [14,16–20] in an effort to re-direct these chimeric toxins to specific cell types. In other instances, domain III has been swapped with other cytotoxic moieties, such as barnase and the ricin A chain [21–23]. Interestingly, the translocating capacity of ETA has never been tested to assess the cytosolic delivery of CPPs or molecular cargos such as polypeptides, drugs or nucleic acids.

Since a limiting step in achieving the full potential of CPP-delivered agents is to facilitate their endosomal escape, we hypothesized that fusing a cationic CPP to the translocation domain of ETA used in designing immunotoxins (residues 253 to 412) [21–23] would favor the efficient internalization of a large molecular cargo and allow it to reach the cytosol. Accordingly, a series of CPP-containing fusion proteins were generated and comparatively tested for their ability to efficiently deliver a large reporter protein, namely the enhanced green fluorescent protein (eGFP), to the cytosol of treated cells.

2. Materials and methods

2.1. Protein constructs

Nucleotide sequences encoding CPP–eGFP (either containing or lacking the $ETA^{253–412}$ coding region) were generated by PCR using primers listed in Supplementary Table 1, and subcloned between the *NcoI/XhoI* or *NdeI/XhoI* restriction sites in a pET15b expression vector (Novagen, San Diego, CA) to generate the fusion proteins listed in Fig. 1. The plasmid containing the DNA coding region for ETA and used as a template to construct the fusion proteins was provided by Dr. A.R. Merrill (Department of Molecular and Cellular Biology, University of Guelph).

The expression of CPP–protein constructs was achieved by growing *E. coli* BL21 (DE3) Star (Invitrogen; Oakville, Ontario, Canada) at 37 °C in lysogeny broth (LB) supplemented with ampicillin (100 μg/mL) while shaking at 250 rpm. At an optical density (OD_{600}) of 0.4–0.6, the expression of fusion proteins was induced using 0.75 mM isopropylthio-β-galactoside (IPTG) for 4–24 h at 37 °C. Cells were sedimented by centrifugation and the corresponding pellets were suspended in a lysis buffer (50 mM Tris pH 8, 500 mM NaCl, 5% glycerol, 0.1% NP-40, 10 mM imidazole) supplemented with Benzonase (1 U/mL Novagen) as well as a cocktail of protease inhibitors (Complete EDTA-free; Roche, Laval, Québec, Canada). The suspended cells were subsequently lysed by sonication and debris were sedimented by centrifugation (12 000 × *g*, 4 °C). The poly-histidine tagged protein constructs, recovered in the supernatant, were purified by affinity chromatography using nickel-NTA agarose resin (Qiagen, Toronto, ON). Bound proteins were washed with wash buffer (50 mM Tris pH 8, 500 mM NaCl, 5% glycerol, 0.1% NP-40, 10 mM imidazole), and eluted using a buffer containing 50 mM Tris pH 8, 500 mM NaCl, and 250 mM imidazole. Solutions of the purified protein constructs were dialyzed against phosphate buffered saline (PBS) using Amicon centrifugal filter devices (Millipore, Bedford, MA). Purity and molecular weight of the recovered proteins were confirmed by SDS-PAGE (Fig. 1B) and mass spectrometry, respectively.

2.2. Cell culture

Human adenocarcinoma cell lines HeLa (cervical carcinoma; ATCC No. CCL-2) and MCF-7 (breast carcinoma; ATCC No. HTB22) were cultured at 37 °C in a humidified 5.0% CO_2 atmosphere in either RPMI 1640 or DMEM H21 media, respectively, supplemented with antibiotics (100 μg/mL penicillin and streptomycin) and 10% heat-inactivated fetal bovine serum (FBS; Wisent Bioproductions, St-Bruno, QC).

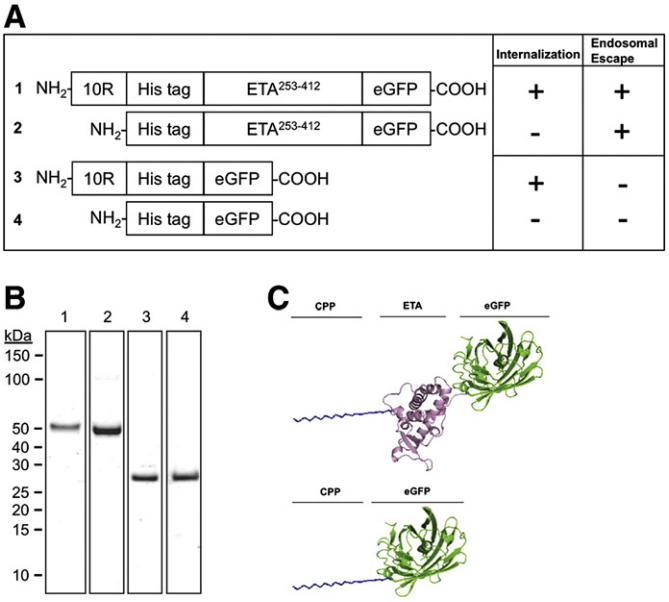

Fig. 1. Summary of recombinant protein constructs used in this study. (A) Schematic representation of CPP protein fusion constructs and their projected capacity for internalization and cytosolic routing. The 10R-His tag–$ETA^{253–412}$–eGFP construct was generated to facilitate protein cargo delivery to the cytosol. The 10R-His tag–eGFP construct served as a control for an imported construct that remained mostly trapped in endosomes while the His tag–$ETA^{253–412}$–eGFP and His tag–eGFP constructs lacking the 10R CPP sequence were negative controls to confirm the need for a CPP peptide in mediating internalization. (B) Coomassie stained SDS-PAGE gel depicting the purity and migration patterns of the protein constructs expressed and purified from *E.coli*. 10R-His tag–$ETA^{253–412}$–eGFP (46.7 kDa; lane 1), His tag–$ETA^{253–412}$–eGFP (46.2 kDa; lane 2), 10R-His tag–eGFP (29.9 kDa; lane 3), and His tag–eGFP (29.2 kDa; lane 4) all ran around their expected molecular weights. (C) Graphical representation of the 10R-His tag–$ETA^{253–412}$–eGFP (top) and 10R-His tag–eGFP (bottom) constructs used in this study and the relative sizes of their domains (CPP and His tag in blue, $ETA^{253–412}$ domain in purple, eGFP domain in green). Images were generated using PyMOL v0.99 (DeLano Scientific LLC, San Francisco, CA).

2.3. Internalization of protein constructs

HeLa cells were seeded (2.5×10^5 cell/mL) and incubated for 16–24 h. To assess the internalization of the different protein constructs, cells were treated with 2 μM of protein constructs diluted in 500 μL growth media and incubated for 1 h at either 4 °C or 37 °C. For ATP depletion studies, cells were incubated at 37 °C with growth media containing 6 mM 2-deoxy-D-glucose (2DDG) and 10 mM NaN_3 for 1 h, and then treated with the protein constructs in the same medium for 1 h at 37 °C [24]. The fluorescence signal arising from eGFP-containing constructs that remained surface bound was quenched using Trypan Blue (0.25 mg/mL) [25,26]. Treated cells were then detached by trypsinization at 37 °C for 5 min and washed three times with PBS supplemented with 2.5% FBS. The internal eGFP fluorescence signal of the cells was then measured by flow cytometry using a FACS Calibur instrument (FL1-H channel, $\lambda_{Ex} = 488$ nm, $\lambda_{Em} = 530$ nm; BD Biosciences, San Jose, CA).

Time-dependent events leading to the internalization and cytosolic delivery of protein constructs were determined by flow cytometry and fluorescence live-cell imaging, respectively. Briefly, HeLa and MCF-7 cells were seeded (2.5×10^5 cells/mL in a 6-well plate for flow cytometry or 5.0×10^4 cells/mL in a 2-chamber slide for fluorescence live-cell imaging) and incubated for 16–24 h. Cells were then treated with 2 μM of protein constructs diluted in complete medium and incubated for 0, 1, 2, 4, 8, or 24 h at 37 °C. The cells were then treated with 10 μM Cell Tracker Orange CMTMR (Invitrogen), quenched with Trypan Blue, and washed three times with warm PBS. Cells were then washed using ice cold PBS and analyzed by flow cytometry.

For fluorescence live-cell imaging, cells incubated in the presence of CPP–protein modules were topped up with complete medium lacking

phenol red and imaged using a Zeiss LSM 700 confocal microscope (Carl Zeiss, Jena, Germany). For the purpose of conducting a comparative study, all imaging parameters (i.e. detector gain, laser power, and pinhole size) were kept constant.

2.4. Quantification of eGFP fluorescence

2.4.1. Mean intracellular eGFP fluorescence intensity

The mean intracellular eGFP fluorescence intensity (MFI) referred to in this text represents the total intracellular eGFP fluorescence signal of cells analyzed by flow cytometry.

2.4.2. Average cytosolic eGFP fluorescence intensity

The average cytosolic eGFP fluorescence intensity referred to in this text represents the eGFP fluorescence signal that overlapped with the CMTMR cytosolic stain signal in each cell analyzed by confocal microscopy. Image Pro Plus 6.3 software (Media Cybernetics, Bethesda, MD) was used to quantify the overlap of eGFP and CMTMR fluorescence signals from the images acquired by confocal microscopy. For measurements, the threshold range was set to exclude background fluorescence. Single cells were gated and the "*Sum of the Intensity Values per pixel*" was measured using the *Count/Size* tool. The average cytosolic eGFP fluorescence intensity in arbitrary units (a.u.) was then calculated using the following equation:

$$\text{Average cytosolic eGFP intensity (a.u.)} = \frac{\text{Total Fluorescence Intensity}}{\text{Number of Cells Measured}}.$$

2.5. Time-dependent changes in the routing of protein cargos to subcellular locations

HeLa cells were seeded and treated with 10R-His tag–ETA$^{253–412}$–eGFP, as described above, followed by staining with Hoechst Dye 33342 (nucleus) and LysoTracker Red DND-99 (Invitrogen; lysosomes). Extracellular fluorescence was quenched using Trypan Blue [25,26].

Staining of the endoplasmic reticulum and early endosome compartments were achieved separately using either CellLight ER-RFP *BacMam 2.0* (RFP-calreticulin/KDEL fusion) or CellLight Early Endosomes-RFP *BacMam 2.0* (RFP-Rab5a fusions; Invitrogen), respectively, as suggested by the manufacturer. Briefly, HeLa cells were seeded and then transduced overnight with 35 viral particles per cell (PPC). The CellLight reagent was washed away with PBS and cells were treated with 10R-His tag–ETA$^{253–412}$–eGFP as described above. The cells were then stained with 5 μg/mL Hoechst Dye 33342 (Invitrogen), quenched with Trypan Blue, washed three times with warm PBS, and topped up with complete medium lacking phenol red. Fluorescence live-cell imaging was performed using a Zeiss LSM 510 META NLO two-photon confocal microscope (Carl Zeiss).

2.6. Inhibition of protein trafficking and translocation

The intracellular routing of CPP–ETA constructs was confirmed by analyzing cells treated with inhibitors of vesicular transport. Specifically, HeLa cells cultured in the presence of 10R-His tag–ETA$^{253–412}$–eGFP for 24 h were treated with either 4 mM NH_4Cl (Sigma-Aldrich) or 7 μM brefeldin A (BFA, BioShop Canada Inc., Burlington, ON, Canada). Untreated cells served as controls. Inhibitor-treated and control cells were examined by flow cytometry and live-cell imaging, as described above.

3. Results and discussion

3.1. Generation of CPP-fused constructs capable of internalizing a macromolecular cargo

Proving the value of the ETA translocation domain in facilitating the routing of proteins to the cytosol of cells required the engineering of non-cytotoxic CPP-tagged constructs capable of efficient internalization. The initial testing of different polycationic CPPs indicated that decaarginine (10R) was an efficient CPP at internalizing cargos (Broad and Gariépy, unpublished observations). Subsequently, a series of 10R-fused constructs were engineered either containing or lacking residues 253 to 412 of ETA (ETA$^{253–412}$) corresponding to domains II and Ib (Fig. 1A). ETA$^{253–412}$ has been frequently used in the design of immunotoxins in the past with domain Ib acting as a spacer between domains II and III [21–23]. Importantly, the assignment of the ETA translocation function to only domain II (residues 253–364) remains speculative as this minimal structural domain has never been analyzed to provide this function in isolation from both domains I and III. In the present constructs, the ETA domain Ib separates domain II from a large protein cargo (eGFP) ensuring that the functionality of the cargo would not be disturbed by the addition of this domain in the construct.

Incubation of HeLa cells for 1 h at 4 °C with 2 μM of all protein constructs did not produce a significant shift in the observed intracellular fluorescence (Fig. 2, panel A), whereas incubation of cells with 10R-containing eGFP fusion proteins at 37 °C led to a marked shift in intracellular eGFP fluorescence (Fig. 2B). As expected, treatment of HeLa cells with constructs lacking an N-terminal CPP (His tag–eGFP and His tag–ETA$^{253–412}$–eGFP) at 37 °C did not result in an increase in the intracellular fluorescence signal measured (Fig. 2B). In contrast, cells exposed to 10R-His tag–eGFP and 10R-His tag–ETA$^{253–412}$–eGFP imported these constructs at 37 °C (Fig. 2B). Importantly, cells treated with 10R-His tag–ETA$^{253–412}$–eGFP exhibited a greater shift in intracellular eGFP fluorescence than cells treated with 10R-His tag–eGFP, supporting the hypothesis that incorporating ETA$^{253–412}$ into a CPP-cargo increases the cytosolic release of the construct thus reducing its degradation or exocytosis via mechanisms associated with endosomal entrapment. Furthermore, when cells were depleted of adenosine triphosphate (ATP) using 2-deoxy-D-glucose (2DDG), a >80% and 60% loss in the mean intracellular fluorescence signals recorded for cells treated with 10R-His tag–ETA$^{253–412}$–eGFP and 10R-His tag–eGFP, respectively, were observed in relation to fluorescence signals observed for cells treated with these constructs at 37 °C in the absence of 2DDG (Fig. 2C). Again, no significant shift in the intracellular fluorescence was seen when cells were treated with CPP-lacking constructs in the presence of 2DDG at 37 °C (Fig. 2C). Taken together, the temperature and ATP depletion data suggest that the internalization of CPP-containing constructs is independent of the presence of the ETA$^{253–412}$ domain and is affected by the fluidity of the cell membrane, as well as the presence of ATP [27–29]. These findings are in agreement with the known import characteristics of cationic CPPs, such as 10R. Mechanistically, polycationic CPPs bind to negatively charged heparin sulfate groups on cell surface proteoglycans (HSPGs), which act as multivalent low affinity receptors that internalize bound CPPs through endocytic pathways such as macropinocytosis or clathrin-mediated endocytosis [1,3]. The effect of protein construct concentration on internalization was also tested and found to positively correlate with the amount of fluorescence signal measured by flow cytometry in HeLa and MCF-7 cells (Supplementary Fig. 1A and B). All subsequent protein internalization and intracellular routing experiments were performed at a protein concentration of 2 μM where cellular toxicity was not observed (Supplementary Fig. 1C).

3.2. Cargo delivery to the cytosol is enhanced by the addition of ETA$^{253–412}$ to 10R-containing protein constructs

The time-dependent internalization of 10R-His tag–ETA$^{253–412}$–eGFP and 10R-His tag–eGFP into cells was evaluated using HeLa and MCF-7 cells treated with these constructs over a 24-hour time period. The mean intracellular eGFP fluorescence intensity (MFI) of the treated cell population(s) was measured by flow cytometry (Fig. 3). Overall, cells treated with the construct containing the CPP and the ETA$^{253–412}$ domain exhibited a greater internalization efficiency in both cell types

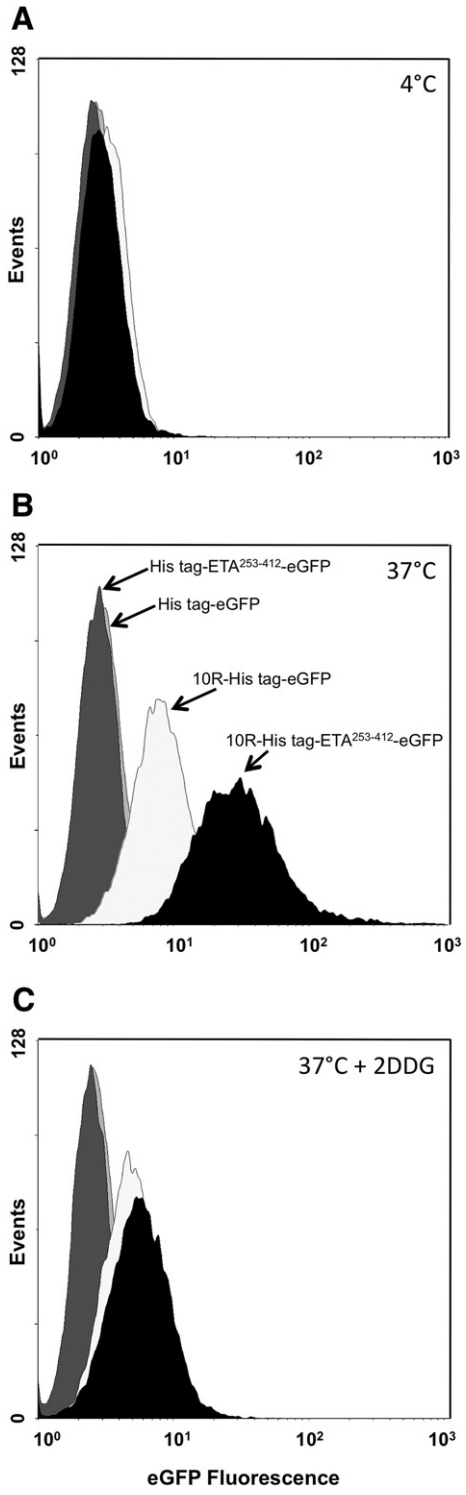

Fig. 2. CPP-containing constructs can internalize their protein cargo in an energy-dependent manner. The eGFP fluorescence in HeLa cells treated with 2 μM of protein constructs for 1 h at 4 °C (panel A), 37 °C (panel B), or 37 °C + ATP depletion with 2-deoxy-D-glucose (2DDG) as described in Materials and methods (panel C) was measured by flow cytometry. Flow analysis was only performed on gated viable cell populations. His tag–eGFP: light gray; His tag–ETA$^{253–412}$–eGFP: dark gray; 10R-His tag–eGFP: white; 10R-His tag–ETA$^{253–412}$–eGFP: black.

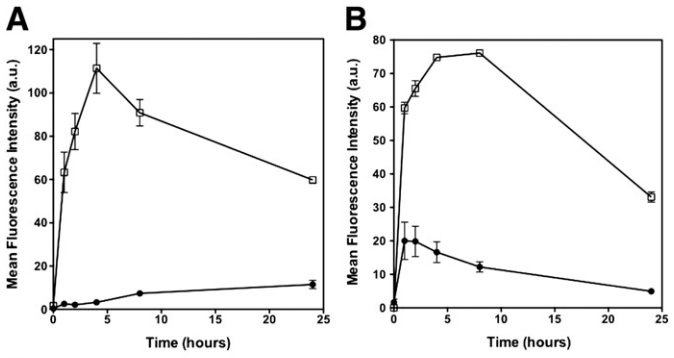

C

	Mean Fluorescence Intensity (a.u.)	
	HeLa	MCF-7
10R-His tag-ETA$^{253-412}$-eGFP	59.8 ± 1.5	33.1 ± 1.5
10R-His tag-eGFP	11.5 ± 1.9	5.0 ± 0.6
P Value	< 0.0001	< 0.0001

Fig. 3. 10R-containing constructs are internalized in a time-dependent manner. Flow cytometry was used to measure the mean eGFP fluorescence intensity (arbitrary units, a.u.) in HeLa cells (A) and MCF-7 cells (B) treated with 2 μM of 10R-His tag–eGFP (black circles) or 10R-His tag–ETA$^{253–412}$–eGFP (open squares) for 0, 1, 2, 4, 8, and 24 h at 37 °C. Each time point represents the average MFI value of an experiment performed 6 times with HeLa cells and 4 times with MCF-7 cells, where 2.5×10^5 cells were analyzed by flow cytometry. Flow analysis was only performed on gated viable cell populations. (C) Table comparing the mean eGFP fluorescence intensities (a.u.) of cells treated with the CPP-fused constructs for 24 h as measured by flow cytometry from panels A and B. MFI values are listed with their respective standard error of the mean (SEM) values. *P* values were calculated using an unpaired *t*-test.

over 24 h resulting in MFI values 5-fold greater than cells treated with construct lacking the ETA$^{253–412}$ translocation domain (Fig. 3). Interestingly, the level of cellular uptake peaked for both cell lines between 4 and 8 h and then regressed slowly following their exposure to the constructs. In contrast, cytoplasmic accumulation was more dominant at 24 h (Fig. 4). The higher intracellular fluorescence signal observed for the construct internalized into cells by 4–8 h as compared to 24 h can be attributed in part to the fact that the construct has not yet reached steady-state levels inside cells in relation to the extracellular concentration of the construct by 4–8 h. As the residual endosome-entrapped construct is degraded or recycled out of cells by 24 h, the cytosolic fluorescence signal component becomes more significant due to accumulation of successfully delivered construct, although the overall fluorescence signal recorded in cells is lower.

To confirm that the incorporation of ETA$^{253–412}$ into CPP-containing modules did indeed result in routing cargos to the cytosol, live cell fluorescence imaging by confocal microscopy was performed on MCF-7 and HeLa cells treated with the CPP-containing constructs and counterstained with the Cell Tracker Orange CMTMR cytosolic stain (red color; Fig. 4). The intracellular distribution of CPP-fused cargos was visualized on live cells only to eliminate artifactual redistribution of CPPs in the cytoplasm and nucleus [28]. Over a 24-hour time course, cells treated with 10R-His tag–eGFP exhibited a sparse punctate fluorescence distribution, suggesting that the internalized construct remains trapped in endocytic vesicles. In contrast, cells treated with 10R-His tag–ETA$^{253–412}$–eGFP displayed a gradual increase in green fluorescence that was within the cell and co-localized with the red-colored cytosolic stain. These changes in eGFP fluorescence signal over time seen by confocal microscopy were quantified by measuring the average cytosolic fluorescence intensity within cells treated with CPP-fused constructs and demonstrated that the incorporation of ETA$^{253–412}$ to 10R-His tag–eGFP resulted in a 40-fold enhancement in protein cargo routing to the cytosol (Fig. 5).

3.3. Characterization of the intracellular routing of ETA$^{253–412}$ fused CPP-constructs

The suggested mechanism by which ETA is routed to the cytosol of intoxicated cells is facilitated by its domain II and requires that the toxin

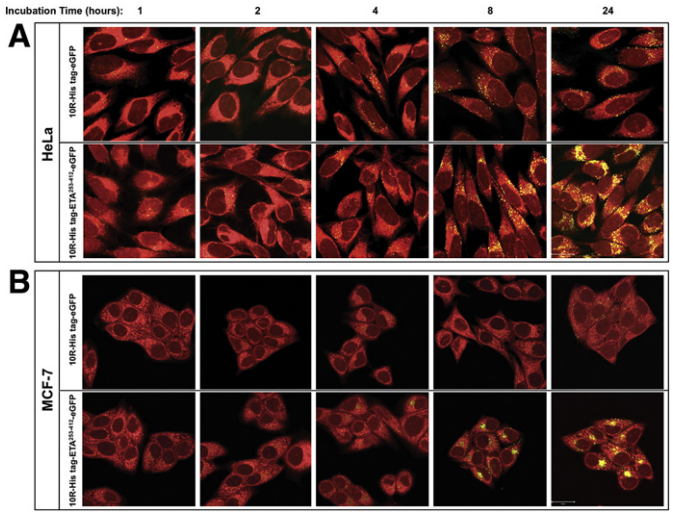

Fig. 4. Incorporation of ETA$^{253–412}$ into 10R-containing constructs improves their cytosolic delivery. HeLa (A) and MCF-7 (B) cells were treated with 2 μM of 10R-His tag–eGFP (green, top panels) or 10R-His tag–ETA$^{253–412}$–eGFP (green, bottom panels) and imaged on live cells by confocal microscopy. Scale bar set at 20 μm. Cytosolic stain (CMTMR) is colored red.

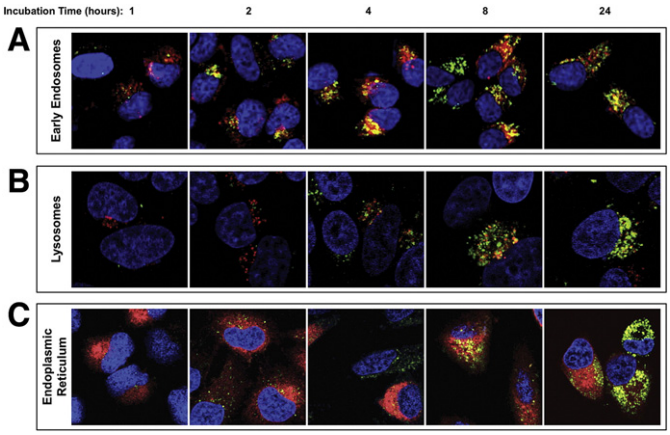

Fig. 6. Incorporating the ETA$^{253–412}$ domain into a CPP-containing eGFP construct facilitates its cytosolic translocation and requires its transit through the ER lumen. HeLa cells were treated with 10R-His tag–ETA$^{253–412}$–eGFP (green) over a 24-hour time course as described in Materials and methods. Early endosomes were labeled using CellLight Early Endosomes-RFP *BacMam 2.0* (red, A), lysosomes were labeled with LysoTracker Red DND-99 (red, B), while the endoplasmic reticulum compartment (ER) was labeled using CellLight ER-RFP *BacMam 2.0* (red, C). Yellow signal indicates co-localization of the 10R-His tag–ETA$^{253–412}$–eGFP construct (in green) and cellular compartments (in red). Nuclei were labeled with Hoechst Dye 33342 (blue).

travels from endosomes to the ER lumen prior to reaching the cytosol [33,34]. To assess if our CPP construct displayed a similar routing mechanism, HeLa cells were treated with 10R-His tag–ETA$^{253–412}$–eGFP and were stained using organelle-specific probes and imaged by confocal microscopy to visualize cellular compartments potentially accessed during the intracellular routing of the ETA-containing CPP-fused constructs into cells over 24 h (Fig. 6).

As depicted in Fig. 6, a transient co-localization of 10R-His tag–ETA$^{253–412}$–eGFP in early endosomes was observed in the first 4 h of treatment, with the highest signal detected at 4 h (Fig. 6, panel A).

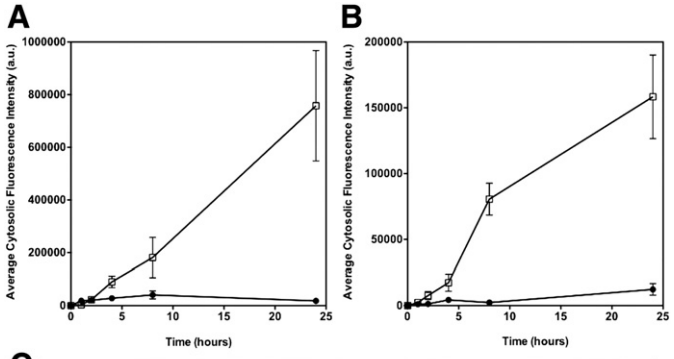

C

	Average Cytosolic Fluorescence Intensity (x10^3, a.u.)	
	HeLa	MCF-7
10R-His tag-ETA$^{253-412}$-eGFP	758 ± 210	158 ± 32
10R-His tag-eGFP	18.1 ± 5.0	12.3 ± 4.4
P Value	0.0012	0.0005

Fig. 5. Incorporating the ETA$^{253–412}$ translocation domain into 10R-containing constructs improves their delivery to the cytosol. The average cytosolic eGFP fluorescence intensity (arbitrary units, a.u.) observed in HeLa cells (A; N = 18) and MCF-7 cells (B; N = 8) treated with 2 μM of either 10R-His tag–eGFP (black circles) or 10R-His tag–ETA$^{253–412}$–eGFP (open squares) over a 24-hour time course. Quantification of cytosolic fluorescence was done using images acquired by confocal microscopy and analyzed by Image Pro Plus 6.3 as described in the Materials and methods section. (C) Table comparing the average cytosolic eGFP fluorescence intensities (a.u.), presented with their SEM values, of cells treated with the CPP-fused constructs for 24 h measured by analysis of images captured by confocal microscopy from panels A and B. *P* values were calculated using an unpaired *t*-test.

Interestingly, no co-localization was observed with lysosomes (Fig. 6, panel B) suggesting that the presence of the ETA$^{253–412}$ domain favors the redistribution of the cargo protein to the cytosol (Fig. 4). This result indicates that the addition of the ETA$^{253–412}$ domain allows its fusion partner to be routed away from endocytic vesicles at a stage preceding the acidification of late endosomes. Finally, labeling the ER lumen of 10R-His tag–ETA$^{253–412}$–eGFP treated cells with a red fluorescent ER lumen-resident protein (BacMam reagent) revealed the transient localization of 10R-His tag–ETA$^{253–412}$–eGFP to this compartment at 4 and 8 h (Fig. 6, panel C), suggesting that 10R-His tag–ETA$^{253–412}$–eGFP routes to the ER lumen prior to relocating to the cytosol. This finding is in agreement with previous reports highlighting the routing of exotoxin A itself from endocytic vesicles and through the ER lumen prior to reaching the cytoplasm via retrograde transport [30,31].

To further validate the observed cellular trafficking pathway taken by 10R-His tag–ETA$^{253–412}$–eGFP, we used inhibitors of intracellular trafficking. Specifically, HeLa cells were pre-treated with 10R-His tag–ETA$^{253–412}$–eGFP and exposed to either ammonium chloride (NH_4Cl), an inhibitor of endosome to lysosome acidification that results in the impairment of receptor-mediated endocytosis [32–35], or brefeldin A (BFA), an antibiotic that disrupts the Golgi apparatus and inhibits trafficking between the ER and the Golgi, as well as the endosomes and lysosomes [34,36–38]. Mean fluorescence intensities were measured using flow cytometry (Fig. 7A), and the addition of NH_4Cl to 10R-His tag–ETA$^{253–412}$–eGFP-treated HeLa cells resulted in a decrease of cytosolic fluorescence intensity to ~15% of the control group and retained a dispersed punctate distribution (green; Fig. 7B), which can be attributed to the reduction of vesicular transport as a result of a reduction of lysosomal acidification; whereas, NH_4Cl treatment essentially had no effect on the mean intracellular fluorescence intensity of HeLa cells pre-treated with 10R-His tag-eGFP (Supplementary Fig. 2). In contrast, the addition of BFA to HeLa cells pre-treated with 10R-His tag–ETA$^{253–412}$–eGFP resulted in a significant reduction of cytosolic fluorescence intensity (Fig. 7). This observation is in accordance with previous studies on ETA where cells pre-treated with BFA were shown to be less sensitive to the action of this toxin [31,34]. Importantly, the brefeldin A treatment results suggest that the Golgi network must be intact for the 10R-His tag–ETA$^{253–412}$–eGFP construct to reach the cytosol. Taken together,

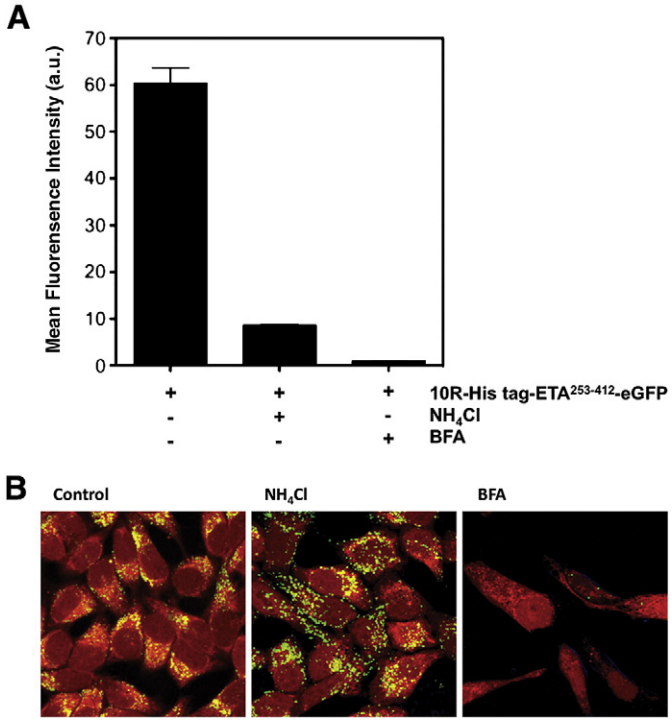

Fig. 7. Prevention of cytosolic translocation of 10R-His tag–ETA$^{253–412}$–eGFP following the inhibition of cellular transport events. Addition of inhibitors of cellular routing events affects the cellular uptake of 10R-His tag–ETA$^{253–412}$–eGFP into HeLa cells. Cells were incubated with the 10R-His tag–ETA$^{253–412}$–eGFP construct (green) and grown in the presence of either 4 mM ammonium chloride (NH_4Cl) or 7 μM brefeldin A (BFA) for 24 h at 37 °C. HeLa cells grown in the absence of inhibitors served as controls for cytosolic translocation. (A) Quantification of the mean intracellular eGFP fluorescence intensity measured by flow cytometry. Flow analysis was only performed on gated viable cell populations. Results represent the average values derived from experiments repeated 3 times. (B) Confocal microscopy images of HeLa cells showing the reduction in co-localization of the construct (green) and the cytosol stain (red) as a result of the retention of internalized CPP constructs in endocytic vesicles (NH4Cl treatment).

these observations suggest that the addition of ETA$^{253–412}$ to the 10R-His tag–eGFP fusion led to the retrograde transport of the construct from early endosomes, through the ER lumen and to the cytosol.

4. Conclusion

The development of effective delivery strategies to route protein therapeutics acting on cytosolic targets remains challenging particularly for proteins being imported using cationic CPP sequences. This study demonstrated the additive effect of incorporating the ETA$^{253–412}$ domain to a CPP-containing protein construct in significantly improving their delivery to the cytosol, while posing no apparent cytotoxicity to treated cells (HeLa and MCF-7). Furthermore, the presented results suggest that the addition of the ETA translocation domain to CPP-containing fusion constructs mediates its transport to the cytosol through its retrograde trafficking from endosomes to the ER lumen, although further studies are required to define the minimal region of ETA necessary for the observed relocalization. Adding a bacterial protein domain (ETA$^{253–412}$ domain) to the design of protein therapeutics is expected to increase their immunogenicity. However, a broad range of immunotoxins, most of which based on the ETA scaffold are presently being evaluated in clinical trials [39] and methods have been proposed to limit the immunogenicity of ETA constructs [39]. Ontak, an IL2-DT immunotoxin is presently used to treat patients with cutaneous T-cell lymphoma [40]. Thus, the concept reported herein provides a promising strategy in designing protein constructs able to relocate to the cytosol of cells, thus addressing one key limiting factor hindering the broader application of cationic CPP-mediated delivery of therapeutic proteins and drugs.

Acknowledgments

This study was funded by grants from the Canadian Breast Cancer Research Alliance and the Canadian Institutes of Health Research (CIHR) to Jean Gariépy. Arshiya F. Mohammed was supported by Ontario Graduate Scholarship and CIHR studentships.

Appendix A. Supplementary data

Supplementary data to this article can be found online at http://dx.doi.org/10.1016/j.jconrel.2012.10.006.

References

[1] G.M. Poon, J. Gariepy, Cell-surface proteoglycans as molecular portals for cationic peptide and polymer entry into cells, Biochem. Soc. Trans. 35 (2007) 788–793.
[2] P.M. Fischer, Cellular uptake mechanisms and potential therapeutic utility of peptidic cell delivery vectors: progress 2001–2006, Med. Res. Rev. 27 (2007) 755–795.
[3] S.M. Fuchs, R.T. Raines, Pathway for polyarginine entry into mammalian cells, Biochemistry 43 (2004) 2438–2444.
[4] R. Fischer, K. Kohler, M. Fotin-Mleczek, R. Brock, A stepwise dissection of the intracellular fate of cationic cell-penetrating peptides, J. Biol. Chem. 279 (2004) 12625–12635.
[5] I.A. Khalil, K. Kogure, S. Futaki, H. Harashima, High density of octaarginine stimulates macropinocytosis leading to efficient intracellular trafficking for gene expression, J. Biol. Chem. 281 (2006) 3544–3551.
[6] K.S. Kawamura, M. Sung, E. Bolewska-Pedyczak, J. Gariepy, Probing the impact of valency on the routing of arginine-rich peptides into eukaryotic cells, Biochemistry 45 (2006) 1116–1127.
[7] J.P. Richard, K. Melikov, H. Brooks, P. Prevot, B. Lebleu, L.V. Chernomordik, Cellular uptake of unconjugated TAT peptide involves clathrin-dependent endocytosis and heparan sulfate receptors, J. Biol. Chem. 280 (2005) 15300–15306.
[8] J.S. Wadia, R.V. Stan, S.F. Dowdy, Transducible TAT-HA fusogenic peptide enhances escape of TAT-fusion proteins after lipid raft macropinocytosis, Nat. Med. 10 (2004) 310–315.
[9] M.Z. Kounnas, R.E. Morris, M.R. Thompson, D.J. FitzGerald, D.K. Strickland, C.B. Saelinger, The alpha 2-macroglobulin receptor/low density lipoprotein receptor-related protein binds and internalizes *Pseudomonas* exotoxin A, J. Biol. Chem. 267 (1992) 12420–12423.
[10] J. Hwang, D.J. Fitzgerald, S. Adhya, I. Pastan, Functional domains of *Pseudomonas* exotoxin identified by deletion analysis of the gene expressed in *E. coli*, Cell 48 (1987) 129–136.
[11] Y. Jinno, M. Ogata, V.K. Chaudhary, M.C. Willingham, S. Adhya, D. FitzGerald, I. Pastan, Domain II mutants of *Pseudomonas* exotoxin deficient in translocation, J. Biol. Chem. 264 (1989) 15953–15959.
[12] D.M. Rasper, A.R. Merrill, Evidence for the modulation of *Pseudomonas aeruginosa* exotoxin A-induced pore formation by membrane surface charge density, Biochemistry 33 (1994) 12981–12989.
[13] M.P. Taupiac, M. Bebien, M. Alami, B. Beaumelle, A deletion within the translocation domain of *Pseudomonas* exotoxin A enhances translocation efficiency and cytotoxicity concomitantly, Mol. Microbiol. 31 (1999) 1385–1393.
[14] A. Kihara, I. Pastan, Analysis of sequences required for the cytotoxic action of a chimeric toxin composed of *Pseudomonas* exotoxin and transforming growth factor alpha, Bioconjug. Chem. 5 (1994) 532–538.
[15] C.B. Siegall, V.K. Chaudhary, D.J. FitzGerald, I. Pastan, Functional analysis of domains II, Ib, and III of *Pseudomonas* exotoxin, J. Biol. Chem. 264 (1989) 14256–14261.
[16] V.K. Chaudhary, D.J. FitzGerald, S. Adhya, I. Pastan, Activity of a recombinant fusion protein between transforming growth factor type alpha and *Pseudomonas* toxin, Proc. Natl. Acad. Sci. U. S. A. 84 (1987) 4538–4542.
[17] D.J. FitzGerald, R. Kreitman, W. Wilson, D. Squires, I. Pastan, Recombinant immunotoxins for treating cancer, Int. J. Med. Microbiol. 293 (2004) 577–582.
[18] R.J. Kreitman, V.K. Chaudhary, T. Waldmann, M.C. Willingham, D.J. FitzGerald, I. Pastan, The recombinant immunotoxin anti-Tac(Fv)-*Pseudomonas* exotoxin 40 is cytotoxic toward peripheral blood malignant cells from patients with adult T-cell leukemia, Proc. Natl. Acad. Sci. U. S. A. 87 (1990) 8291–8295.
[19] R.J. Kreitman, I. Margulies, M. Stetler-Stevenson, Q.C. Wang, D.J. FitzGerald, I. Pastan, Cytotoxic activity of disulfide-stabilized recombinant immunotoxin RFB4(dsFv)-PE38 (BL22) toward fresh malignant cells from patients with B-cell leukemias, Clin. Cancer Res. Off. J. Am. Assoc. Cancer Res. 6 (2000) 1476–1487.
[20] R.K. Puri, D.S. Hoon, P. Leland, P. Snoy, R.W. Rand, I. Pastan, R.J. Kreitman, Preclinical development of a recombinant toxin containing circularly permuted interleukin 4 and truncated *Pseudomonas* exotoxin for therapy of malignant astrocytoma, Cancer Res. 56 (1996) 5631–5637.
[21] C. Pitcher, L. Roberts, S. Fawell, A.G. Zdanovsky, D.J. FitzGerald, J.M. Lord, Generation of a potent chimeric toxin by replacement of domain III of *Pseudomonas* exotoxin with ricin A chain KDEL, Bioconjug. Chem. 6 (1995) 624–629.
[22] T.I. Prior, D.J. FitzGerald, I. Pastan, Translocation mediated by domain II of *Pseudomonas* exotoxin A: transport of barnase into the cytosol, Biochemistry 31 (1992) 3555–3559.

[23] T.I. Prior, S. Kunwar, I. Pastan, Studies on the activity of barnase toxins in vitro and in vivo, Bioconjug. Chem. 7 (1996) 23–29.
[24] M. Mano, C. Teodosio, A. Paiva, S. Simoes, M.C. Pedroso de Lima, On the mechanisms of the internalization of S4(13)-PV cell-penetrating peptide, Biochem. J. 390 (2005) 603–612.
[25] S. Deshayes, T. Plenat, G. Aldrian-Herrada, G. Divita, C. Le Grimellec, F. Heitz, Primary amphipathic cell-penetrating peptides: structural requirements and interactions with model membranes, Biochemistry 43 (2004) 7698–7706.
[26] M. Foley, A.N. MacGregor, J.R. Kusel, P.B. Garland, T. Downie, I. Moore, The lateral diffusion of lipid probes in the surface membrane of *Schistosoma mansoni*, J. Cell Biol. 103 (1986) 807–818.
[27] G. Drin, S. Cottin, E. Blanc, A.R. Rees, J. Temsamani, Studies on the internalization mechanism of cationic cell-penetrating peptides, J. Biol. Chem. 278 (2003) 31192–31201.
[28] J.P. Richard, K. Melikov, E. Vives, C. Ramos, B. Verbeure, M.J. Gait, L.V. Chernomordik, B. Lebleu, Cell-penetrating peptides. A reevaluation of the mechanism of cellular uptake, J. Biol. Chem. 278 (2003) 585–590.
[29] P. Saalik, A. Elmquist, M. Hansen, K. Padari, K. Saar, K. Viht, U. Langel, M. Pooga, Protein cargo delivery properties of cell-penetrating peptides. A comparative study, Bioconjug. Chem. 15 (2004) 1246–1253.
[30] D.C. Smith, R.A. Spooner, P.D. Watson, J.L. Murray, T.W. Hodge, M. Amessou, L. Johannes, J.M. Lord, L.M. Roberts, Internalized *Pseudomonas* exotoxin A can exploit multiple pathways to reach the endoplasmic reticulum, Traffic 7 (2006) 379–393.
[31] J.E. Weldon, I. Pastan, A guide to taming a toxin—recombinant immunotoxins constructed from *Pseudomonas* exotoxin A for the treatment of cancer, FEBS J. 278 (2011) 4683–4700.
[32] G. Misinzo, P.L. Delputte, H.J. Nauwynck, Inhibition of endosome–lysosome system acidification enhances porcine circovirus 2 infection of porcine epithelial cells, J. Virol. 82 (2008) 1128–1135.
[33] L.I. Simpson, The binary toxin produced by *Clostridium botulinum* enters cells by receptor-mediated endocytosis to exert its pharmacologic effects, J. Pharmacol. Exp. Ther. 251 (1989) 1223–1228.
[34] T. Yoshida, C.C. Chen, M.S. Zhang, H.C. Wu, Disruption of the Golgi apparatus by brefeldin A inhibits the cytotoxicity of ricin, modeccin, and *Pseudomonas* toxin, Exp. Cell Res. 192 (1991) 389–395.
[35] K. Kim, N.B. Groman, Mode of inhibition of diphtheria toxin by ammonium chloride, J. Bacteriol. 90 (1965) 1557–1562.
[36] O. Garred, E. Dubinina, A. Polesskaya, S. Olsnes, J. Kozlov, K. Sandvig, Role of the disulfide bond in Shiga toxin A-chain for toxin entry into cells, J. Biol. Chem. 272 (1997) 11414–11419.
[37] J. Lippincott-Schwartz, L. Yuan, C. Tipper, M. Amherdt, L. Orci, R.D. Klausner, Brefeldin A's effects on endosomes, lysosomes, and the TGN suggest a general mechanism for regulating organelle structure and membrane traffic, Cell 67 (1991) 601–616.
[38] A. Nebenfuhr, C. Ritzenthaler, D.G. Robinson, Brefeldin A: deciphering an enigmatic inhibitor of secretion, Plant Physiol. 130 (2002) 1102–1108.
[39] M. Onda, R. Beers, L. Xiang, B. Lee, J.E. Weldon, R.J. Kreitman, I. Pastan, Recombinant immunotoxin against B-cell malignancies with no immunogenicity in mice by removal of B-cell epitopes, Proc. Natl. Acad. Sci. U. S. A. 108 (2011) 5742–5747.
[40] G. Manoukian, F. Hagemeister, Denileukin diftitox: a novel immunotoxin, Expert Opin. Biol. Ther. 9 (2009) 1445–1451.